PCCP

ROYAL SOCIETY OF CHEMISTRY

PAPER

Published on 18 March 2026
Licence and permissions

Cite this: *Phys. Chem. Chem. Phys.*, 2026, **28**, 8487

Intermetallic reaction and eutectic transitions tune the reactivity in core–shell Mg/Ni nanoparticles

Mahbub Chowdhury,†[a] Lei Yang,†[a] Brandon Wagner,[b] Yuxin Zhou,[a] Lorenzo Mangolini*[b] and Michael R. Zachariah*[a]

Received 26th November 2025,
Accepted 11th February 2026

DOI: 10.1039/d5cp04582g

rsc.li/pccp

There is developing interest in tuning interfaces to manipulate the performance and safety of energetic materials comprising metallic fuels. One approach is to employ a core–shell architecture to trigger pre-ignition reactions. Here, we investigated the dynamic interfacial reactions and diffusion pathways of synthesized nickel-coated magnesium nanoparticles with sub-nanometer spatial and millisecond temporal resolution under controlled heating by *in situ* TEM, complemented by *ex situ* reactivity characterization. Upon heating, outward diffusion of Mg into the Ni shell forms an intermediate Mg_2Ni phase, directly evidenced by TEM diffraction. This highly exothermic alloying rapidly elevated particle temperature, initiated eutectic melting at the Mg–Ni interface, and accelerated completion of outward Mg transport at temperatures well below those of uncoated Mg. By tuning the Ni-shell thickness, we reduced the ignition temperature by up to ~200 °C. Overall, our study provides valuable insights into the development of designing energetic materials with safer operation and precisely controlled energy release.

Introduction

Nanoscale metals have long been explored as reactive components in energetic systems due to their high surface area and rapid oxidation kinetics.[1–7] However, this strategy of reducing particle size comes with inherent trade-offs, including a reduction in active content caused by the increased mass fraction of the passivating native oxide.[1] Additionally, fine particles are prone to sintering and agglomeration at elevated temperatures, which limits combustion efficiency.[8–10] Among metal fuels, magnesium (Mg) stands out as a lightweight, high-energy-density material with a high enthalpy of combustion and unique vaporization behavior, making it an attractive candidate for propulsion and pyrotechnic applications.[11,12] Nevertheless, Mg combustion is governed by a diffusion-limited process in which Mg vapor must pass through a native oxide shell.[13,14] Although the oxide is partially permeable, it imposes a significant kinetic barrier that delays ignition and reduces reaction rates in practical systems.[15]

To address these limitations, surface modification strategies have been applied to metal nanoparticles (NPs) to tailor their oxidation behavior and improve energy release characteristics.[16–22] In aluminum-based systems, a variety of coatings, including organic passivants, fluorinated compounds, and inorganic shells, have been used to enhance both stability and combustion performance.[16–22] In particular, metal–metal core–shell designs, such as Ni-coated or Cu-coated aluminum nanoparticles, provide additional exothermic alloying reactions at the interface; thereby enhancing reaction rates and lowering ignition temperatures.[16,17,23] Despite these advances in aluminum-based materials, relatively little attention has been given towards similar surface engineering approaches for Mg. Hydrogenation has been shown to be an effective way to lower the ignition temperature of Mg by up to ~200 °C.[24] Recent work by Wagner and co-workers demonstrated that Si–SiO_x coated Mg nanoparticles exhibit significantly improved ignition behavior, with ignition temperatures reduced from 740 °C to 520 °C compared to uncoated Mg.[3] Other approaches, such as paraffin or siloxane coatings, have primarily focused on improving oxidation resistance in air, often at the expense of combustion performance.[25,26] These findings suggest that core–shell architectures represent a promising pathway to improve the ignition and combustion properties of Mg, but further exploration is needed.

Here, we report the synthesis and characterization of nickel-coated magnesium (Ni-coated Mg) nanoparticles as a new route to enhance the reactivity of Mg-based fuels. Ni was chosen as the shell material due to its high thermal conductivity and its ability to form exothermic intermetallic compounds with Mg.[27] Furthermore, the Mg–Ni binary system exhibits a eutectic melting point of 506 °C,[28] lower than the melting point of pure Mg (650 °C), which promotes early phase transitions and facilitates Mg vaporization during ignition.[28] Ni-coated Mg

[a] *Departments of Chemical Engineering and Materials Science, University of California, Riverside, California 92521, USA. E-mail: mrz@engr.ucr.edu*
[b] *Department of Material Science and Engineering, University of California, Riverside, California 92521, USA. E-mail: lmangolini@engr.ucr.edu*
† Mahbub Chowdhury and Lei Yang contributed equally to this work.

nanoparticles were synthesized using a two-stage process involving thermal evaporation of Mg followed by solution-phase Ni coating. We characterized the morphology, structure, and surface chemistry of the resulting core–shell particles and investigated their combustion performance in the presence of Bi_2O_3 as a primary oxidizer. Our findings reveal that the Ni shell significantly lowers the ignition temperature and accelerates combustion, an effect that we attribute to a synergy between early eutectic melting and interfacial alloying reactions.

Experimental

Synthesis of Mg nanoparticles

Magnesium nanoparticles were synthesized by thermal evaporation. Briefly, 250 mg of bulk Mg precursor was resistively heated in high-purity argon flowing at 350 sccm. The chamber pressure was maintained at 40 Torr. An 80-A current was applied to a MeiVac Re-Vap evaporation head (900 W). Under these conditions, Mg nanoparticles with an average diameter of ~210 nm were produced. Particles were collected downstream on a stainless-steel mesh filter. To prevent ignition, a small amount of air was slowly introduced at the outlet to passivate the particles before removal. A schematic of the experimental setup is shown in Fig. 1a.

Ni functionalization of Mg nanoparticles

The as-synthesized Mg nanoparticles were coated with Ni *via* solution-phase reduction. First, the particles were dispersed by ultrasonic agitation in Dimethylformamide (DMF) solvent containing $NiCl_2{\cdot}6H_2O$ (Alfa Aesar, 99.95%). A DMF solution of excess NH_3BH_3 (Sigma-Aldrich, 90%) was then added to reduce Ni^{2+} onto the Mg surfaces. The sealed mixture was maintained in a 40 ± 2 °C water bath with continuous ultrasonic agitation for 80 min (Fisher Scientific FS30D; cooling water added every 20 min). The product was washed with DMF (to quench further nucleation and remove impurities) and isolated by centrifugation (10^4 rpm, 10 min).

Elemental analysis (ICP-OES)

Elemental compositions were quantified by microwave-assisted acid digestion followed by inductively coupled plasma optical emission spectroscopy (ICP-OES). Powder (5 mg) was weighed into Teflon digestion vessels and digested using a MiniWAVE microwave module (SCP Science; 6 × 75 mL configuration). Each sample was dissolved in concentrated HNO_3 (70%) and HCl (35%). Vessels were sealed and heated at full power for 20 min with a pressure set point of 70 psi. After cooling, digests were diluted with Milli-Q water and analyzed by ICP-OES (PerkinElmer Optima 7300DV). External calibration standards were included to ensure analytical accuracy.

TEM measurements

All the TEM analysis were performed with an FEI Titan Themis 300 equipped with an X-FEG electron gun source, operating at 300 kV under a vacuum of 10^{-7} torr.

In situ TEM experiments were conducted using a protochips fusion holder system. The samples were prepared by drop casting solution of the powdered material dispersed in hexane, onto a holey carbon film. The temperature was precisely controlled and monitored *via* the Fusion AX system allowing for well-defined thermal conditions during real-time observations. High-resolution TEM (HRTEM) experiments were performed by heating samples from room temperature to 430 °C at 60 °C min^{-1} to quantitatively compare the diffusion flux between the Ni-coated Mg and control Mg samples. High-magnification images were recorded throughout the process to track the intermediate lattice changes. Fast Fourier transforms (FFTs) of lattice images were generated using ImageJ software. These patterns were indexed by comparison with simulated diffraction patterns derived from SingleCrystal Software.

High-angle annular dark field (HAADF) imaging, in conjunction with energy-dispersive X-ray spectroscopy (EDS), was implemented to capture real-time diffusion behavior. For this analysis, a slower heating rate of 10 °C min^{-1} was employed with isothermal holds of 1 min at each set point. EDS spectra were acquired during each hold to capture real-time diffusion behavior under well-defined thermal conditions.

T-Jump/TOFMS and ignition characterization

Rapid heating and ignition measurements were performed using a temperature jump/time-of-flight mass spectrometry (T-Jump/TOFMS) system at a heating rate of 10^5 °C s^{-1}. A detailed description of the instrument is available in our prior work.[29] Briefly, stoichiometric nanothermite powder was first dispersed in hexane and sonicated to ensure uniform dispersion. The mixture was then uniformly coated onto a platinum wire (1-cm length, 76-μm diameter, OMEGA Engineering Inc.) The coated wire was then pulse-heated for 3 ms at 10^5 °C s^{-1}. Evolved gaseous species were ionized by 70-eV electron gun and detected by a multichannel plate detector for 10 ms at a sampling interval of 0.1 ms. The temperature of the Pt wire was determined by measuring the current across the wire using a Teledyne LeCroy CP040A current probe, and the wire temperature was determined from the current-temperature relationship using the Callender-Van Dusen equation.

TGA-DSC and XRD

Thermogravimetric and differential scanning calorimetric analyses (TGA-DSC) were conducted on a NETZSCH STA 449 F3 Jupiter, using a heating rate of 10 °C min^{-1}. X-ray diffraction (XRD) was performed on a PANalytical Empyrean Series 2 diffractometer with Cu K_α radiation to assess phase composition and crystallinity.

Results and discussion

Mg–MgO core–shell nanoparticles were synthesized *via* thermal evaporation (Fig. 1a), as previously reported.[3] The resulting nanoparticles consist of a mixture of hexagonal plate-like, pyramidal, and bipyramidal shapes (Fig. S1) consistent with

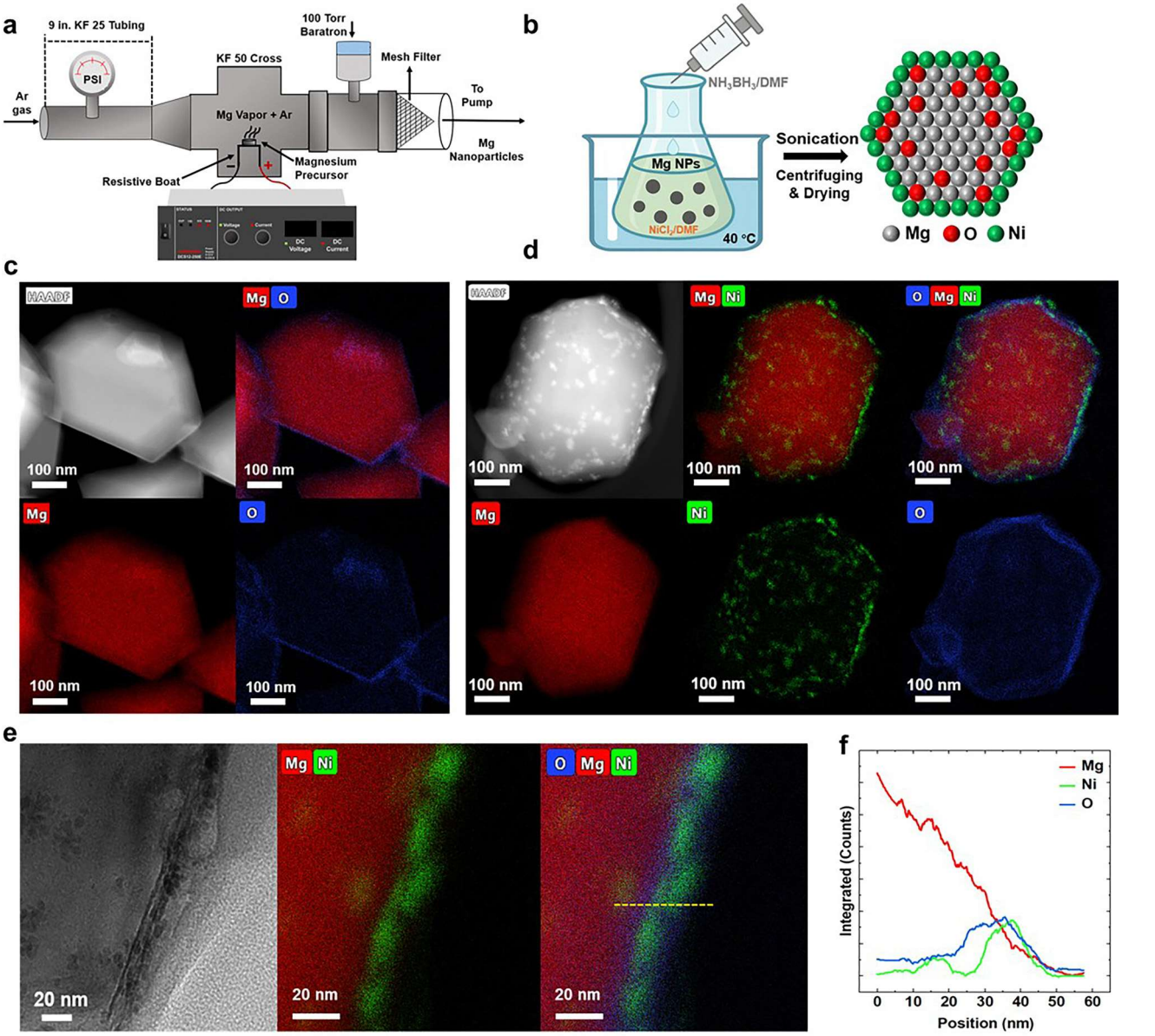

Fig. 1 (a) Schematic of the thermal evaporation process used to produce Mg nanoparticles. (b) Functionalization of Mg surfaces with a Ni coating *via* a solution-based method. (c) STEM–EDS images of core–shell Mg/MgO particles synthesized by thermal evaporation. (d) Core–shell Ni-coated Mg nanoparticles after surface modification. (e) High-resolution TEM image with corresponding STEM–EDS mapping, showing the Ni-coated Mg core–shell structure. (f) EDS line-scan signals of Mg, Ni, and O, showing the Ni shell thickness.

our previous studies.[3,14,24] The average particle size was ~210 nm, and the corresponding particle size distribution is shown in Fig. S1. The collected particles were subsequently subjected to a surface modification process to nucleate Ni on the MgO shell, as illustrated in Fig. 1b, following the reaction:

$$2NiCl_2 + NH_3BH_3 \rightarrow 2Ni(s) + NH_4BCl_4 + H_2(g) \quad (1)$$

STEM–EDS analysis (Fig. 1c) confirmed the presence of a uniform oxide shell on the uncoated Mg particles. A high-resolution image of the Ni-coated Mg nanoparticles is provided in Fig. S2. The functionalization process performed with a Mg : Ni molar ratio of 1 : 0.04 successfully produced a Ni coating of approximately 10 nm in thickness (Fig. 1d and e). A representative EDS line scan is shown in Fig. 1f. The ratio between Mg and Ni was measured with inductively coupled plasma optical emission spectroscopy (ICP-OES). To further tailor the reactivity, an additional, thicker Ni coating was applied using a Mg : Ni molar ratio of 1 : 0.22, producing a shell thickness of ~35 nm (Fig. S3).

The ignition behavior of Ni-coated Mg particles was evaluated and compared with unmodified Mg nanoparticles using temperature-jump ignition, temperature-jump time-of-flight mass spectrometry (T-Jump TOFMS), and high-speed imaging (Fig. 2a). Fuel samples (uncoated Mg and Ni-coated Mg) were incorporated into nanothermite composites by mixing them

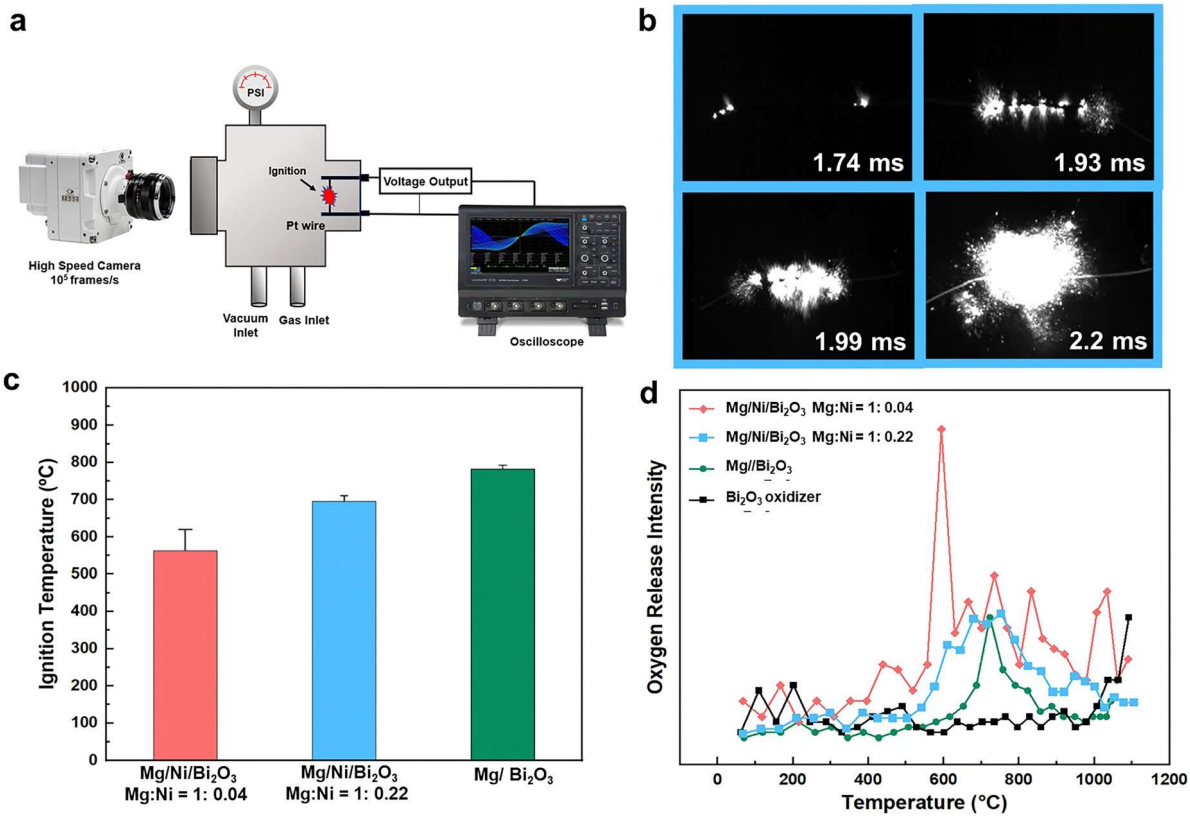

Fig. 2 (a) Schematic of the T-Jump ignition setup. (b) High-speed imaging snapshots showing the ignition sequence of Ni-coated Mg (Mg : Ni = 1 : 0.22) nanoparticles mixed with Bi_2O_3. (c) Comparison of ignition temperatures for Ni-coated Mg nanoparticles and uncoated Mg nanoparticles, determined *via* T-Jump ignition tests. (d) Oxygen release profiles from T-Jump time-of-flight mass spectrometry (TOFMS), comparing coated, uncoated, and neat Bi_2O_3 samples.

with stoichiometric amounts of Bi_2O_3, which served as the oxidizer. The composites were rapidly heated at a rate of $\sim 10^5$ °C s^{-1} for ~3 ms, and the ignition temperature was determined based on the onset of optical emission captured by high-speed imaging. The ignition snapshots of Ni-coated Mg are shown in Fig. 2b.

The uncoated Mg/Bi_2O_3 composite exhibited a significantly higher ignition temperature (~780 ± 10 °C) compared to both thin (~560 ± 50 °C) and thick coated (~690 ± 10 °C) Ni–Mg samples (Fig. 2c). Interestingly, the thick Ni-coating resulted in a higher ignition temperature than the thin coating. This is likely due to the thicker Ni layer acting as a diffusion barrier, which impedes the transport of Mg to the oxidizer. This ~220 °C reduction in ignition temperature can be compared with other surface modification methods previously employed for Mg, such as Si/SiOx coatings (~220 °C) and hydrogenation of Mg particles (~200 °C).[3,29] One advantage of using a Ni coating is that it can substantially reduce the eutectic melting point, as will be discussed in detail.

T-Jump TOFMS further validated these findings by monitoring oxygen release from Bi_2O_3 during heating (Fig. 2d). The neat Bi_2O_3 oxidizer (without fuel) did not show significant oxygen release until temperatures above 1000 °C, consistent with our previous studies.[14] In contrast, the thin-coated Ni–Mg sample exhibited oxygen release near ~560 °C, closely corresponding to its ignition temperature. The thick-coated sample showed delayed oxygen release, consistent with its elevated ignition temperature.

Differential scanning calorimetry (DSC) was performed at a heating rate of 10 K min^{-1} under an ultrahigh-purity argon atmosphere. The experiment was interrupted at 550 °C to allow for X-ray diffraction (XRD) characterization of the intermediate products. For the control Mg sample, a sharp endothermic peak was observed at ~650 °C (Fig. 3a), corresponding to the melting of pure magnesium. In contrast, both Ni-coated Mg samples showed a distinct exothermic peak at significantly lower temperatures, indicating a condensed-phase alloying reaction at the Mg-Ni interface. XRD analysis of the quenched sample at 550 °C confirmed the formation of Mg_2Ni, with characteristic diffraction peaks at 20.2° and 45.3°, corresponding to the (1 0 −1) and (2 0 −3) planes, respectively (Fig. 3b).

The exothermic alloying event was immediately followed by an endothermic peak at ~450–545 °C for Ni-coated Mg samples. These peaks correspond to eutectic melting in the Mg–Ni system (as shown in Fig. S4, phase diagram calculated with Thermo-Calc software, which occurs well below the melting point of pure Mg (~650 °C). Table 1 summarizes the enthalpies associated with key thermochemical processes during heating. DSC measured a heat release of 52.56 J g^{-1} at a composition

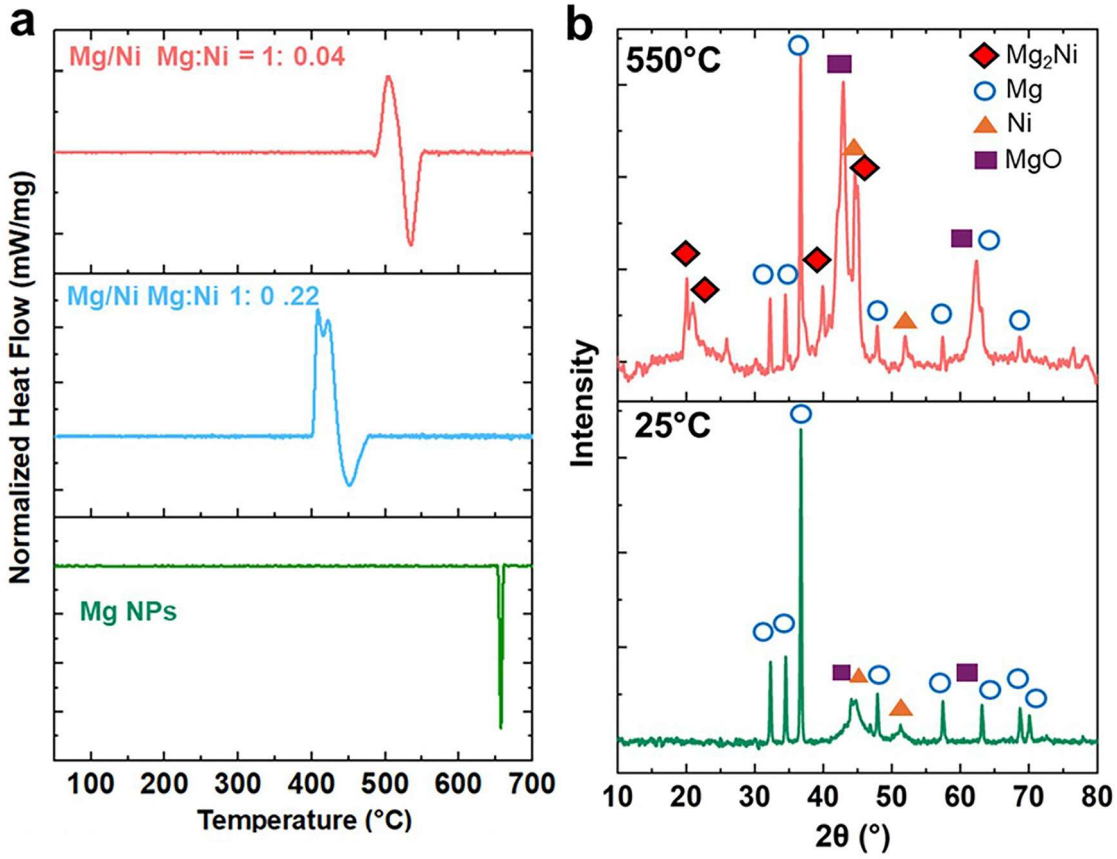

Fig. 3 (a) Differential scanning calorimetry (DSC) profiles of Ni-coated Mg particles measured in ultra-high-purity argon at 10 K min^{-1}, showing exothermic alloying peaks followed by melting behavior. (b) XRD patterns of Mg/Ni samples heated to 550 °C, compared with the unheated sample, confirming the formation of the Mg_2Ni alloy as a result of the alloying reaction.

Table 1 Thermochemical processes during the heating of nickel-coated Mg nanoparticles

Event	Temperature	Thermochemical Processes	ΔH° (kJ mol^{-1})
Mg alloying reaction	410–510 °C	2Mg (s) + Ni (s) → Mg_2Ni (s)	−60[30]
Eutectic melting	450–540 °C	Mg (s) + Mg_2Ni (s) → Mg (l) + Mg_2Ni (s)	8.4[31]

with a 0.22 Ni mol fraction. This value was compared with the theoretical heat release of 124.5 J g^{-1} expected for complete Mg_2Ni formation, indicating that ∼42.2% of the available Ni participated in the alloying reaction. Detailed thermal calculations are provided in the SI.

The heat released during the alloying reaction was sufficient to overcome the enthalpy of fusion of Mg and raise the particle temperature by ∼120 °C, thereby enabling earlier melting of the Mg core. It is interesting to note that untreated Mg must rely primarily on diffusion through the MgO barrier before significant reaction can occur which slows down the kinetics. On the other hand, even though the nickel shell is not atomically uniform around Mg particle, this heat-assisted melting mechanism directly contributes to the reduced ignition temperature observed in the T-Jump ignition experiments, as the exothermic alloying reaction promotes accelerated Mg vaporization and facilitates combustion initiation at lower temperatures.

Finally, we conducted *in situ* heating experiments on Ni-coated Mg nanoparticles using high-resolution TEM at a heating rate of 60 °C min^{-1}. During heating, outward diffusion of Mg was observed, resulting in hollowing of the particles (Fig. 4a and b). The complete diffusion sequence and flux calculations are provided in the SI. For the control Mg sample, the onset of Mg diffusion occurred at ∼360 °C, with complete diffusion observed within a ∼10 °C interval (Fig. 4e). In contrast, Ni-coated Mg nanoparticles exhibited an earlier onset of diffusion ∼300 °C, though the process is considerably slower due to Mg diffusing outward through the Ni shell.

High-magnification TEM images were collected to investigate the *in situ* formation of Mg_2Ni following outward diffusion of Mg. Fig. 4c shows lattice fringes corresponding to (003) and (200) crystal planes of Mg_2Ni. These planes intersect at a 90° angle, agreeing with the theoretically expected relationship of hexagonal Mg_2Ni. Fast Fourier Transform (FFT) analysis was performed further on the corresponding HRTEM region.

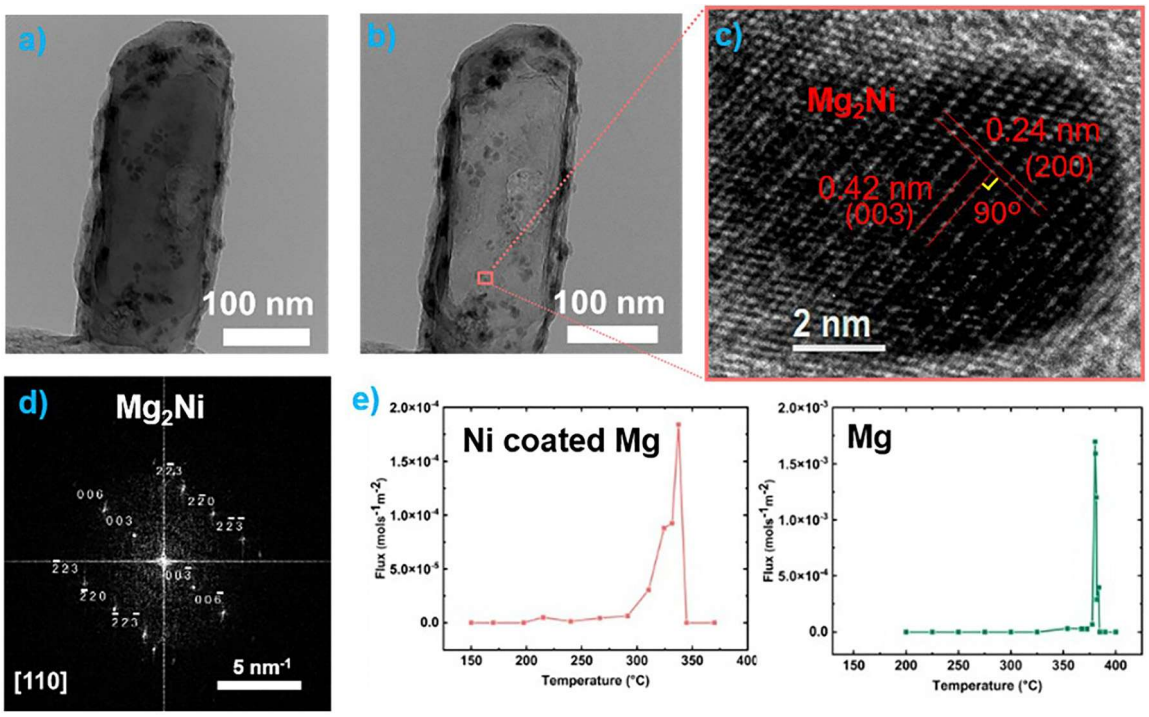

Fig. 4 *In situ* TEM heating of Ni-coated Mg nanoparticles at a rate of 1 K s^{-1} (a) before heating (b) after heating, showing outward diffusion of Mg and particle hollowing. (c) HRTEM images from the boxed region, with lattice fringes assigned to Mg_2Ni (200) and (003), showing the formation of the intermediate Mg_2Ni phase from alloying reaction (d) Corresponding fast Fourier transform (FFT) pattern of the HRTEM region indexed to [110] zone axis (e) Comparison of diffusion flux during heating, showing earlier onset of Mg diffusion in Ni-coated Mg compared to the control Mg sample.

The resulting diffraction pattern (Fig. 4d) was indexed directly by comparing with the simulated pattern generated using SingleCrystal software. The experimental FFT demonstrated good agreement with the simulated [110] zone axis pattern of Mg_2Ni. The combination of measured d-spacing, angular relationships, and FFT pattern confirms the successful *in situ* formation of Mg_2Ni intermetallic phase.

The formation of Mg_2Ni releases significant heat (~ -60 kJ mol^{-1}), which locally elevates the particle temperature. Furthermore, the nucleation of Mg_2Ni lowers the eutectic melting point to ~ 505 °C.[32] This lowering of melting point promotes earlier outward diffusion of Mg from the Ni-coated sample, as seen from Fig. 4e. It should also be noted that *in situ* TEM heating experiments can introduce additional electron-beam heating, which may raise the local particle temperature by as much as ~ 200 °C consistent with previous studies.[33–36] Furthermore, the high vacuum ($\sim 10^{-7}$ Torr) in the TEM chamber lowered the vaporization temperature of Mg. This effect provides an additional explanation for the earlier onset of Mg diffusion observed in TEM compared to TGA measurements and ignition experiments.

We also conducted *in situ* heating experiments on Ni-coated Mg nanoparticles using TEM equipped with STEM-EDS at a slow heating rate of 10 °C min^{-1} to observe the diffusion of Mg from the core into the Ni shell. At room temperature, prior to heating, Mg was confined within both the thick (Fig. 5a) and thin Ni shell (Fig. S5). Upon heating, Mg was observed to diffuse outward from the core, resulting in a semi-hollow structure. Corresponding EDS spectra revealed overlapping signals of Mg and Ni at the particle interface (Fig. 5b), confirming the formation of Mg-Ni intermetallic compounds, consistent with XRD analysis and earlier *in situ* TEM observations. The porous nature of the native MgO shell likely facilitates both outward diffusion of Mg and inward diffusion of Ni, promoting intermetallic formation at the core–shell interface.

A schematic summary of the ignition mechanism of Mg diffusion in Ni-coated Mg nanoparticles is shown in Fig. 5c. Previous studies suggest that at elevated temperatures, Mg in Ni–Mg alloys tends to segregate to the surface, driven by both the atomic size mismatch between Ni and Mg and the difference in their surface energies. When Mg_2Ni alloys are in proximity to an oxidizer such as Bi_2O_3, oxygen ions can diffuse into the alloy, initiating a process known as chemisorption-induced segregation.[37] Upon oxygen exposure at elevated temperatures, the alloy surface begins to decompose: Mg diffuses outward toward the surface, while Ni remains enriched in the near-surface region. This outward Mg migration shortens the diffusion distance between Mg and Bi_2O_3, thereby enhancing reaction kinetics. Simultaneously, oxygen diffuses inward, establishing bidirectional diffusion pathway.

As oxygen penetrates the alloy matrix, it leads to the oxidation of Mg_2Ni *via* Mg segregation and NiO formation as reported by *in situ* XPS study conducted under oxygen-rich conditions.[37] In this state, outwardly diffusing Mg can react not only with Bi_2O_3 but also with NiO formed *in situ*, creating additional exothermic reaction pathways that further facilitate

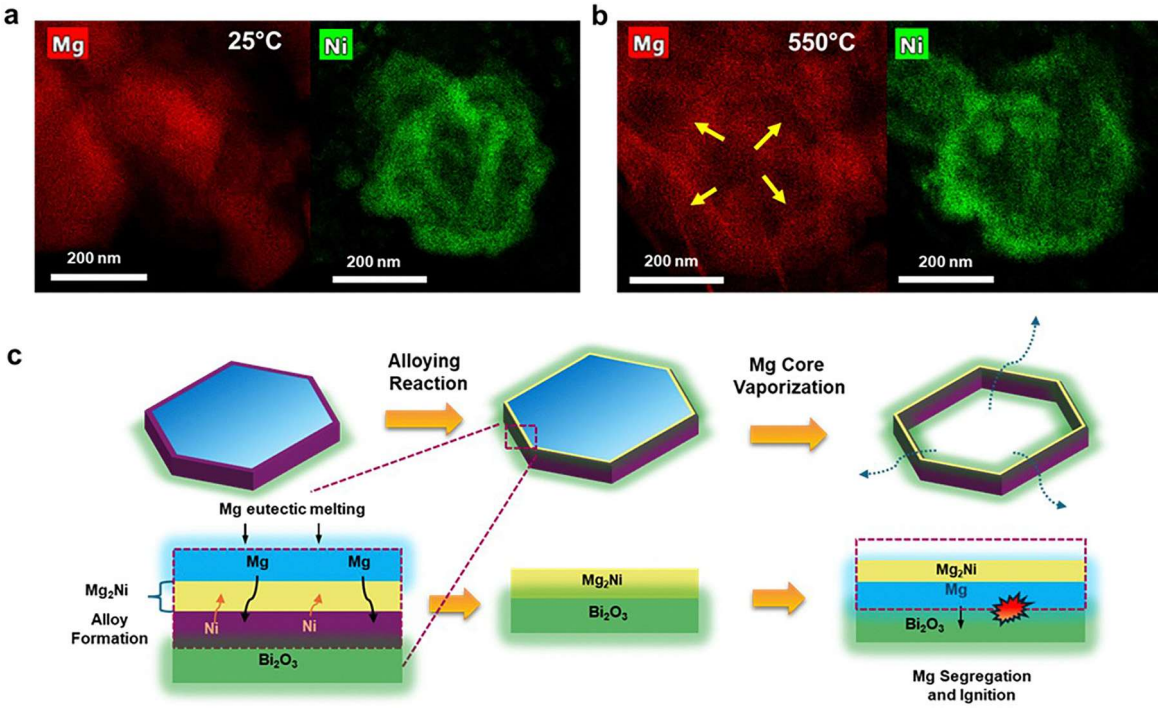

Fig. 5 *In situ* heating STEM-EDS of Ni-coated Mg particles under vacuum. (a) Images at room temperature showing the initial Mg–Ni core–shell structure. (b) Images at elevated temperatures showing Mg diffusion into the Ni shell, providing evidence of alloy formation at the interface. (c) Proposed schematic of the reaction mechanism.

ignition and combustion. We performed additional DSC tests (Fig. S6) to rule out the possibility of Ni reacting with Bi_2O_3. Upon heating, we did not observe any exothermic peaks, indicating minimal reaction between Ni and Bi_2O_3 under our conditions.

$$Mg + NiO \rightarrow MgO + Ni\ \Delta H_r = -362\ kJ\ mol^{-1} \quad (2)$$

$$3Mg + Bi_2O_3 \rightarrow 3MgO + 2Bi\ \Delta H_r = -1227\ kJ\ mol^{-1} \quad (3)$$

Thus, the combined effects of the exothermic alloying reaction, the lowering of the eutectic melting point, and the interfacial reactions of segregated Mg with both oxidized Ni and the external oxidizer (Bi_2O_3) collectively contribute to a substantial reduction in ignition temperature. This synergy between structural evolution, heat release, and interfacial chemistry provides a tunable pathway to significantly enhance ignition performance.

Conclusions

In summary, we developed core–shell Ni-coated Mg particles using a two-step process that combines vapor-phase synthesis of Mg nanoparticles with solution-phase Ni deposition for surface modification. We demonstrated that the ignition temperature of Mg can be significantly tuned by adjusting the thickness of the Ni coating. DSC, XRD, and *in situ* TEM confirmed the formation of Mg_2Ni, which releases substantial heat, raises the particle temperature by up to 120 °C, and promotes early eutectic melting, thereby enhancing Mg mobility toward the oxidizer, Bi_2O_3. T-jump measurements demonstrated that with coating the ignition temperature could be reduced as low as ~200 °C. This is consistent with T-jump mass spectrometry results, which revealed a significantly earlier onset of oxygen release due to accelerated particle heating. Overall, this work highlights the potential of tailoring combustion behavior through controlled intermetallic formation and phase transitions in core–shell nanostructures.

Author contributions

Mahbub Chowdhury: conceptualization, investigation, writing – original draft, methodology, visualization, formal analysis Lei Yang: conceptualization, investigation, writing – original draft, methodology, visualization, formal analysis Brandon Wagner: methodology, investigation Yuxin Zhou: methodology, investigation, conceptualization. Lorenzo Mangolini: supervision, writing – review & editing, conceptualization. Michael R. Zachariah: conceptualization, writing – review & editing, supervision, resources, project administration, methodology, funding acquisition.

Conflicts of interest

There are no conflicts to declare

Data availability

The data supporting this article has been included as part of the article and supplementary information (SI). Supplementary information is available. See DOI: https://doi.org/10.1039/d5cp04582g.

Acknowledgements

This work was supported by the AFOSR and NSF.

References

1 D. Sundaram, V. Yang and R. A. Yetter, Metal-based nanoenergetic materials: synthesis, properties, and applications, *Prog. Energy Combust. Sci.*, 2017, **61**, 293–365.
2 M. Comet, C. Martin, F. Schnell and D. Spitzer, Nanothermites: a Short Review. Factsheet for Experimenters, Present and Future Challenges, *Propellants, Explos., Pyrotech.*, 2019, **44**, 18–36.
3 B. Wagner, P. Ghildiyal, P. Biswas, M. Chowdhury, M. R. Zachariah and L. Mangolini, In-Flight Synthesis of Core–Shell Mg/Si–SiO_x Particles with Greatly Reduced Ignition Temperature, *Adv. Funct. Mater.*, 2023, **33**, 2212805.
4 R. A. Yetter, G. A. Risha and S. F. Son, Metal Particle Combustion and Nanotechnology, *Proc. Combust. Inst.*, 2009, **32**, 1819–1838.
5 S. H. Kim and M. R. Zachariah, Enhancing the Rate of Energy Release from Nanoenergetic Materials by Electrostatically Enhanced Assembly, *Adv. Mater.*, 2004, **16**, 1821–1825.
6 E. L. Dreizin, Metal-based reactive nanomaterials, *Prog. Energy Combust. Sci.*, 2009, **35**, 141–167.
7 A. W. Tomich, S. Proctor, M. Y. Yang, J. Chen, Y. Zhao, E. Chen, T. Das, B. V. Merinov, W. A. I. Goddard, J. Guo and V. Lavallo, Combustion Resistant Borohydrides and Their Chemical Interactions with Li-Metal Surfaces: An Experimental and Theoretical Study, *ACS Cent. Sci.*, 2025, **11**, 734–741.
8 P. Chakraborty and M. R. Zachariah, Do Nanoenergetic Particles Remain Nano-Sized during Combustion?, *Combust. Flame*, 2014, **161**, 1408–1416.
9 N. Zohari, M. H. Keshavarz and S. A. Seyedsadjadi, The Advantages and Shortcomings of Using Nano-Sized Energetic Materials, *Cent. Eur. J. Energy Mater.*, 2013, **10**, 135–147.
10 K. T. Sullivan, N. W. Piekiel, C. Wu, S. Chowdhury, S. T. Kelly, T. C. Hufnagel, K. Fezzaa and M. R. Zachariah, Reactive Sintering: An Important Component in the Combustion of Nanocomposite Thermites, *Combust. Flame*, 2012, **159**, 2–15.
11 C. K. Law and F. A. Williams, Combustion of magnesium particles in oxygen-inert atmospheres, *Combust. Flame*, 1974, **22**, 383–405.
12 R. Lomba, S. Bernard, P. Gillard, C. Mounaïm-Rousselle, F. Halter, C. Chauveau, T. Tahtouh and O. Guézet, Comparison of Combustion Characteristics of Magnesium and Aluminum Powders, *Combust. Sci. Technol.*, 2016, **188**, 1857–1877.
13 I. Shancita, N. G. Vaz, G. D. Fernandes, A. J. A. Aquino, D. Tunega and M. L. Pantoya, Regulating magnesium combustion using surface chemistry and heating rate, *Combust. Flame*, 2021, **226**, 419–429.
14 P. Ghildiyal, P. Biswas, S. Herrera, F. Xu, Z. Alibay, Y. Wang, H. Wang, R. Abbaschian and M. R. Zachariah, Vaporization-Controlled Energy Release Mechanisms Underlying the Exceptional Reactivity of Magnesium Nanoparticles, *ACS Appl. Mater. Interfaces*, 2022, **14**, 17164–17174.
15 L. T. DeLuca, F. Maggi, S. Dossi, M. Fassina, C. Paravan and A. Sossi, in *Chemical Rocket Propulsion: A Comprehensive Survey of Energetic Materials*, ed L. T. De Luca, T. Shimada, V. P. Sinditskii and M. Calabro, Springer International Publishing, Cham, 2017, pp. 191–233.
16 J. Zhang, F. Zhao, H. Li, Z. Yuan, M. Zhang, Y. Yang, Q. Pei, Y. Wang, X. Chen and Z. Qin, Improving Ignition and Combustion Performance of Al@Ni in CMDB Propellants: Effect of Nickel Coating, *Chem. Eng. J.*, 2023, **456**, 141010.
17 L. Yang, Y. Zhou, M. Chowdhury, Y. Qin, M. M. Dickson and M. R. Zachariah, Synergistic transition multi-metal coatings drive sub-melting-point reaction of aluminum, *Chem. Eng. J.*, 2025, **519**, 164794.
18 C. Wang, X. Zou, S. Yin, J. Wang, H. Li, Y. Liu, N. Wang and B. Shi, Improvement of Ignition and Combustion Performance of Micro-Aluminum Particles by Double-Shell Nickel-Phosphorus Alloy Coating, *Chem. Eng. J.*, 2022, **433**, 133585.
19 Y. Jiang, Y. Wang, J. Baek, H. Wang, J. L. Gottfried, C.-C. Wu, X. Shi, M. R. Zachariah and X. Zheng, Ignition and Combustion of Perfluoroalkyl-Functionalized Aluminum Nanoparticles and Nanothermite, *Combust. Flame*, 2022, **242**, 112170.
20 Y. Jiang, H. Wang, J. Baek, D. Ka, A. H. Huynh, Y. Wang, M. R. Zachariah and X. Zheng, Perfluoroalkyl-Functionalized Graphene Oxide as a Multifunctional Additive for Promoting the Energetic Performance of Aluminum, *ACS Nano*, 2022, **16**, 14658–14665.
21 R. Ali, F. Ali, A. Zahoor, R. N. Shahid, N. U. H. Tariq, G. Ali, S. Ullah, A. Shah and H. B. Awais, Preparation and Oxidation of Aluminum Powders with Surface Alumina Replaced by Iron Coating, *J. Energ. Mater.*, 2022, **40**, 243–257.
22 Z. Cheng, X. Chu, J. Yin, B. Dai, W. Zhao, Y. Jiang, J. Xu, H. Zhong, P. Zhao and L. Zhang, Formation of Composite Fuels by Coating Aluminum Powder with a Cobalt Nanocatalyst: Enhanced Heat Release and Catalytic Performance, *Chem. Eng. J.*, 2020, **385**, 123859.
23 Y. Zhou, L. Yang, A. K. Vasudevan, M. Dickson, M. Chowdhury, K. Shi and M. R. Zachariah, Nickel-coated aluminum nanoparticles for modulating ignition temperature: Interfacial chemistry and mechanism, *ACS Appl. Eng. Mater.*, 2025, **3**, 2346–2353.
24 M. Chowdhury, B. Wagner, Y. Wang, K. Shi, I. Tran, M. M. Dickson, L. Mangolini and M. R. Zachariah, Energetic Characteristics and Reaction Mechanism of Hydrogenated Magnesium Nanoparticles: The Role of Condensed-Phase Reaction, *ACS Appl. Mater. Interfaces*, 2025, **17**, 21180–21188.
25 D. L. Hastings, M. Schoenitz, K. M. Ryan, E. L. Dreizin and J. W. Krumpfer, Stability and Ignition of a Siloxane-Coated Magnesium Powder, *Propellants, Explos., Pyrotech.*, 2020, **45**, 621–627.
26 S. Zhang, Coating of magnesium powder by rapid expansion of supercritical solution method, *Trans. Nonferrous Met. Soc. China*, 2006, **16**, s285–s288.
27 H. Zhang, S. Shang, J. E. Saal, A. Saengdeejing, Y. Wang, L.-Q. Chen and Z.-K. Liu, Enthalpies of formation of

magnesium compounds from first-principles calculations, *Intermetallics*, 2009, **17**, 878–885.
28 A. A. Nayeb-Hashemi and J. B. Clark, The Mg–Ni (Magnesium–Nickel) system, *Bull. Alloy Phase Diagrams*, 1985, **6**, 238–244.
29 G. Jian, L. Zhou, N. W. Piekiel and M. R. Zachariah, Low Effective Activation Energies for Oxygen Release from Metal Oxides: Evidence for Mass-Transfer Limits at High Heating Rates, *ChemPhysChem*, 2014, **15**, 1666–1672.
30 H. Zhang, S. Shang, J. E. Saal, A. Saengdeejing, Y. Wang, L.-Q. Chen and Z.-K. Liu, Enthalpies of formation of magnesium compounds from first-principles calculations, *Intermetallics*, 2009, **17**, 878–885.
31 R. N. Abdullaev, A. Sh Agazhanov, A. R. Khairulin, D. A. Samoshkin and S. V. Stankus, Thermophysical Properties of Magnesium in Solid and Liquid States, *J. Eng. Thermophys.*, 2022, **31**, 384–401.
32 Z. Tang, L. Yang, T. Wang, L. Wu, Y. Ma, H. Yan, C. Liu and W. Liu, Interface microstructure regulation and bonding performance of powder metallurgy Al/Mg bimetal with Ni interlayer, *J. Mater. Sci.*, 2023, **58**, 5848–5864.
33 Z. Li, Q. Yin, W. Lv, J. Shen, S. Wang, T. Zhao, J. Cai, H. Lei, S. Lin, Y. Zhang and B. Shen, Electron-Assisted Generation and Straight Movement of Skyrmion Bubble in Kagome $TbMn_6$ Sn_6, *Adv. Mater.*, 2024, **36**, 2309538.
34 B. Aizenshtein and L. Etgar, *In Situ* Intrinsic Self-Healing of Low Toxic Cs_2 ZnX_4 (X = Cl, Br) Metal Halide Nanoparticles, *Small*, 2024, **20**, 2305755.
35 Y. Han, L. Wang, K. Cao, J. Zhou, Y. Zhu, Y. Hou and Y. Lu, *In Situ* TEM Characterization and Modulation for Phase Engineering of Nanomaterials, *Chem. Rev.*, 2023, **123**, 14119–14184.
36 T. Yokota, M. Murayama and J. M. Howe, *In situ* Transmission-Electron-Microscopy Investigation of Melting in Submicron Al–Si Alloy Particles under Electron-Beam Irradiation, *Phys. Rev. Lett.*, 2003, **91**, 265504.
37 P. Stefanov, XPS study of surface segregation in Ni–Mg alloy films, *Vacuum*, 1996, **47**, 1107–1110.